High-yield fabrication of entangled photon emitters for hybrid quantum networking by high temperature droplet epitaxy

Francesco Basso Basset,[*,†,‡] Sergio Bietti,[†] Marcus Reindl,[‡] Luca Esposito,[†] Alexey Fedorov,[¶] Daniel Huber,[‡] Armando Rastelli,[‡] Emiliano Bonera,[†] Rinaldo Trotta,[*,‡] and Stefano Sanguinetti[†,¶]

†*L-NESS and Dipartimento di Scienza dei Materiali, Università degli Studi di Milano-Bicocca, Via Cozzi 55, I-20125 Milano, Italy*

‡*Institute of Semiconductor and Solid State Physics, Johannes Kepler University, Altenbergerstraße 69, Linz 4040, Austria*

¶*L-NESS and CNR-IFN, via Anzani 42, I-22100 Como, Italy*

E-mail: f.bassobasset@campus.unimib.it; rinaldo.trotta@jku.at

Abstract

Several semiconductor quantum dot technologies have been investigated for the generation of entangled photon pairs. Among the others, droplet epitaxy enables control of the shape, size, density, and emission wavelength of the quantum emitters. However, the fraction of entanglement-ready quantum dots that can be fabricated with this method is still limited to values around 5%, and matching the energy of the entangled photons to atomic transitions - a promising route towards quantum networking - remains an outstanding challenge.

Here, we overcome these hurdles by introducing a modified approach to droplet epitaxy on a high symmetry (111)A substrate, where the fundamental crystallization step

is performed at a significantly higher temperature as compared to previous reports. Our method improves drastically the yield of entanglement-ready photon sources near the emission wavelength of interest, which can be as high as 95% thanks to the low values of fine structure splitting and radiative lifetime, together with the reduced exciton dephasing offered by the choice of GaAs/AlGaAs materials. The quantum dots are designed to emit in the operating spectral region of Rb-based slow-light media, providing a viable technology for quantum repeater stations.

Keywords

Quantum dots, entanglement, droplet epitaxy, fine structure splitting, rubidium, resonant two-photon excitation

Under the ongoing effort to develop practical quantum technologies, the search for a suitable entangled photon source is an active research direction, as it plays a role in key quantum communication protocols and some approaches to quantum computation.[1,2] Above all, it is a fundamental requirement for the realization of repeaters capable to transfer quantum entanglement over long distances.

Epitaxial quantum dots (QDs) are a promising alternative to parametric down-converters, given their ability to generate photons on-demand with high efficiency and their compatibility with semiconductor foundries.[3,4] In order to use QD entanglement resources in real-life technologies, two main roadblocks have to be overcome. The first is related to the difficulty of consistently finding emitters capable to generate highly entangled photon pairs. The second concerns the wavelength of operation of the quantum source, which must be compatible with other components of a quantum network, such as storage media and detectors. In this work, we search for the best approach to face these challenges.

In order to achieve reproducible entangled photon generation, it is necessary to deal with the in-plane anisotropies in the confinement potential that induce a fine structure splitting (FSS) between the bright exciton states through electron-hole exchange interaction.[5,6]

Moreover, methods to alleviate exciton dephasing caused by the fluctuating magnetic fields produced by the QD nuclei have be taken into account.[7]

Dephasing by nuclear magnetic fields depends mainly on the material choice. Among the various systems proposed up to now,[6,8–13] GaAs QDs stand out as the best option. In contrast to standard In(Ga)As QDs obtained by the Stranski-Krastanow method, they are weakly affected by exciton spin scattering thanks to low nuclear magnetic moment. Indeed, a recent report[14] has shown unprecedented high levels of entanglement and indistinguishability in photon pairs generated from GaAs/AlGaAs nanostructures fabricated by droplet etching.

Here we want to draw the attention to a different growth strategy based on droplet epitaxy (DE). The DE method for the fabrication of QDs is based on the sequential deposition, at controlled temperature and flux, of group III (Ga, In, Al), to form nano-droplets on the surface, and of group V (As, P, Sb, N), to crystallize the droplets into nano-islands.[15] This technique presents some appealing advantages as compared to droplet etching, that are much wider control over the spatial density of emitters[16] and their shape.[17] Moreover, this growth scheme is compatible with different materials, so that it can be employed to fabricate emitters on a broad spectral range, notably also in the conventional telecom band.[18,19]

GaAs QDs grown by DE have already proved to yield polarization-entangled photons with a very high value of fidelity,[20] without temporal post-selection or external tuning.[21–24] This was made possible by collectively improving the in-plane symmetry of as-grown QDs by means of fabrication on a (111)-oriented substrate.[25,26] Despite the high potential of the fabrication method, DE is still quite far from meeting fundamental requirements for the practical realization of a hybrid semiconductor-atomic quantum network. First, the average value of FSS is still too high and brings to a minority fraction - around 5% - of entanglement-ready emitters, so that finding one with good performance requires time-consuming and large-area scans. In addition to that, it would be desirable to have the emission wavelength matched with an atomic-based optical slow medium, Rb being the natural choice for the GaAs/AlGaAs system.[27] Through control of shape and barrier composition, we aim to reduce

the confinement potential and achieve a practical density of single photon emitters around 780 nm. When this requirement is satisfied, a weak external field can be used to tune the exciton emission within the hyperfine splitting of the ^{87}Rb D_2 transitions to achieve the delay or storage of a polarization qubit.[23,27–29] Finally, a long-standing drawback of this growth technique is the low substrate temperature during formation of the nanostructures and the surrounding barrier. This puts a limit on the crystalline and optical quality of the material, which can only be partially overcome with the help of an annealing process.[30,31]

Research in this direction has only taken its first steps on (111)-grown samples[32] and here we address all these issues by introducing a DE-QDs growth regime where the substrate temperature during the Ga droplet crystallization by As supply is increased by more than 300°C with respect to previous reports.[9,17]

Extensive high resolution single dot spectroscopy experiments revealed reduced spectral wandering and successful control over the emission wavelength. We finally obtained a higher than 95% fraction of the QDs emitting in the strategical wavelength range that shows compliance with the criteria for polarization-entangled photon generation. This is mainly due to a very low average value of FSS and fast radiative recombination. The demonstration of polarization-entangled photon emission is achieved via a two-photon resonant excitation scheme, which is employed here for the first time on DE nanostructures.

Samples of *Ga droplets and* GaAs QDs were fabricated on a GaAs (111)A substrate and embedded in an AlGaAs barrier. The detailed growth procedures and sample structures are reported in the Samples fabrication section. First, metallic Ga nanodroplets are deposited in absence of As supply and, then, they are crystallized into GaAs with the help of the rapid exposure to an intense As flux. In the conventional DE process, the crystallization of the Ga droplets into tridimensional QDs is achieved by keeping under control Ga diffusion length through substrate temperature and As pressure (low T and high As flux), so as to reduce the probability of Ga atoms migrating out of the droplet and binding to As adsorbed by the surrounding AlGaAs surface. Therefore, distinctive feature of this procedure has been

the low temperature required for the crystallization step, around 200°C. The further the temperature is increased, the more planar growth of GaAs on AlGaAs becomes dominant, because it is thermodynamically favorable. In a recent paper,[17] we investigated this process in detail on standard (100) substrates and showed that island formation is observed up to 250°C.

In this work, we present a different quantum dot fabrication regime by DE, in which Ga droplets are crystallized and the subsequent barrier layer is deposited at high substrate temperature, close to the temperature of 520°C which is used for the growth of high quality GaAs and AlGaAs on (111)A. This is expected to improve the crystallinity of the QDs by reducing the concentration of point defects typical for low temperature growth.[30,33] These defects are likely to cause spectral wandering and act as non-radiative recombination channels.[31]

This regime becomes accessible thanks to the specific choice of (111)A substrate orientation. The reason why (111)A surface permits the crystallization under As supply of the Ga nano-droplets into QDs lies in the extremely shorter surface lifetime of As_4, with respect to the usual (001) surface.[34] The low As residence time limits the reactivity of the surface towards the bulk incorporation of the Ga adatoms that detach from the droplet perimeter during the crystallization step. Around 500°C the surface reactivity is low enough to strongly limit the two dimensional growth around the droplet by Ga diffusion and to allow a large part of the Ga stored in the droplet to crystallize in place via vapor-liquid-solid mechanism, by way of direct incorporation of As into the droplet, supersaturation and precipitation at the droplet/substrate interface.[35]

The growth parameters were optimized to obtain a low density of emitters suitable for single dot studies together with a size tailoring to achieve emission around the target wavelength of Rb atomic resonances. *The droplet sample was characterized by AFM. Control over droplet formation leads to a density of the Ga droplets of* 9.1×10^8 cm^{-2}*. The droplets are spherical caps with mean base diameter of 50.4 nm, mean height of 7.4 nm. The volume of the deposited gallium matches the volume of the droplets.*

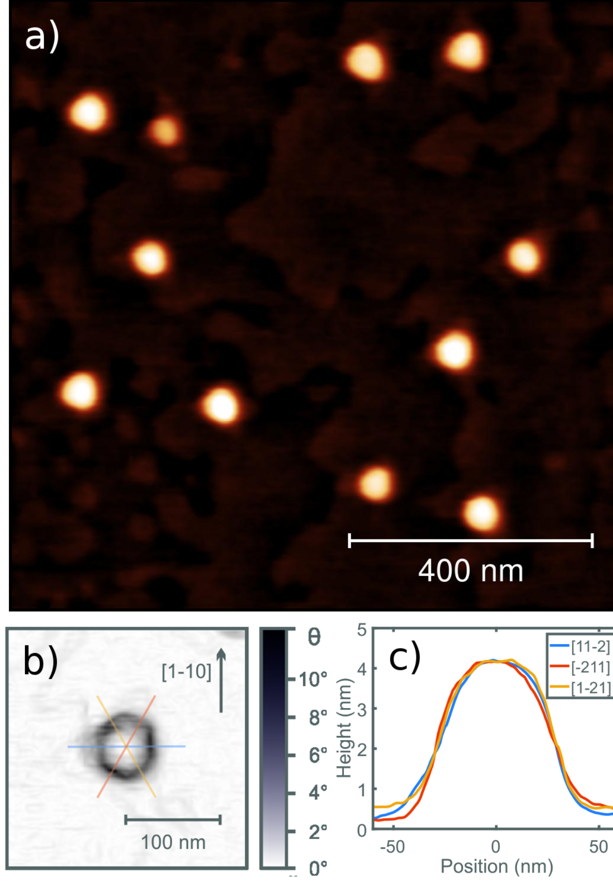

Figure 1: AFM scan of QD *sample. a) 1 μm × 1 μm map* b) 2D map of the inclination angle θ with respect to the (111)A plane. c) Height profiles taken along [11-2] and equivalent crystallographic directions, following the colored lines in panel a).

The formation of nanocrystals *after the crystallization step* was assessed by AFM on uncapped samples. The density of QDs is *in good agreement with the one observed on the droplet sample and equal to* 8.3×10^8 cm^{-2}. *Also the volume of the each nanostructure, taking into account the transformation of liquid Ga in GaAs crystal, is preserved without a signicative change.* While keeping a high substrate temperature, the As flux during crystallization was adjusted in order to result in the desired geometry of the QDs. A quite large size, with a mean base diameter and height of 70 and 4 nm respectively, and a low Al content in the barrier layer were employed to shift excitonic lines at longer wavelengths as compared to previous attempts.[9]

Fig. 1 reports the typical morphology of a nanostructures right after crystallization. *The*

base of the nanosctructures is hexagonal as shown in panel (a). In deeper details, from the map of surface inclination in panel (b), a hexagonal truncated pyramid shape is observed. A different color scale (shown in Supporting Information) would also reveal the presence of a very thin broader triangular base, which is likely due to As incorporation outside the droplet, close to its perimeter. Where the Ga adatom concentration is high enough,[36] layer-by-layer growth is promoted despite the low residence time of As atoms. Fig. 1(c) shows mid-section height profiles collected across three directions that are equivalent according to C_{3v} symmetry. The comparison highlights a high degree of in-plane symmetry.

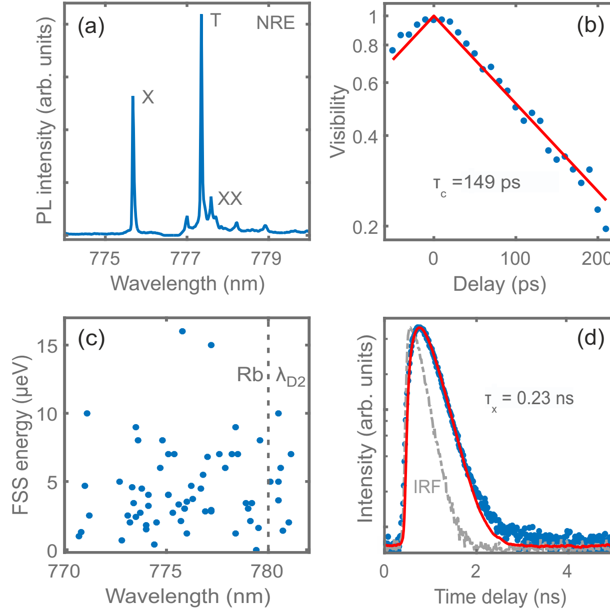

Figure 2: a) Emission spectrum of a single QD under above-barrier excitation. b) Interference visibility of a neutral exciton line from a selected QD (blue dots) fitted with an exponential decay (red continuous line). c) FSS values measured on several QDs emitting at different wavelengths. d) Time decay of the exciton PL emission (blue dots) fitted (red continuous line) with an exponential decay convoluted with the instrument response function (IRF, gray dashed line)

A direct assessment of the optical quality and the investigation of the electronic structure of these nanostructures required an in-depth analysis by means of single dot PL.

Figure 2(a) shows a typical emission spectrum of our QDs under above-barrier excitation. It consists of an intense and isolated line, attributed to the recombination of the neutral

excitons (X), accompanied by a few partially overlapping emissions at higher wavelengths. These lines come from other excitonic complexes with positive binding energies, namely the singly charged excitons (T) and the biexciton (XX), together with other charged multiexcitonic states. The main peaks in the spectrum are labeled according to polarization-resolved measurements. This attribution is also supported by a power-dependence analysis (see Supporting Information) and it is consistent with previous experimental studies[37] as well as with atomistic many-body pseudopotential calculations[38] for GaAs/AlGaAs DE QDs.

Contributions from several multiexcitonic complexes persist even at moderate and low exciting powers, possibly because a deep potential barrier in a weak lateral confinement regime leads to a large number of confined levels, hence a high probability to find a carrier in an excited state or an extra charge captured by tunneling from energetically aligned defect states. An effective negative QD charging may strongly reduce the number of useful biexciton-exciton recombination events, as recent observations on pyramidal $In_{0.25}Ga_{0.75}As$ QDs suggest.[39] The presence of a few multiexcitonic peaks spectrally overlapping has already been reported for GaAs/AlGaAs nanostructures emitting at similar wavelengths, but grown with a different epitaxial technique.[40] However, it has also been shown that the biexciton radiative recombination can be selectively pumped by resorting to resonant excitation schemes.[14] This solution can be successfully applied to our DE QDs, as we will discuss later.

The linewidth of the neutral exciton line at low temperature is usually broadened by spectral diffusion.[41] While this contribution is in practice hard to suppress completely, we observed narrow emission lines on samples with 15% Al content in the barrier and 500°C temperature for the droplet crystallization. A top barrier thickness above 100 nm is crucial to suppress spectral diffusion from fluctuating surface charges.[42] We report that the majority of the neutral exciton lines have a linewidth below the resolution of the experimental setup (40 μeV).

In order to overcome the limited spectral resolution, we performed a series of coherence time measurements by means of a Michelson interferometer. Several neutral exciton lines

were investigated and an example of the visibility decay as a function of time delay is shown in Fig. 2(b). The data are well reproduced by a model which assumes a Lorentzian line broadening, even if a Gaussian contribution due to spectral wandering is always present, as commonly reported under above-barrier excitation.[43,44] The Lorentzian fit immediately yields the exciton coherence time which can be easily translated in terms of spectral broadening.[45] We report an average exciton zero-phonon linewidth of 15 μeV and a best value of 9 μeV, which is an improvement over the state of the art for DE QDs[31,32] that amounts to 35 μeV. This result can be most likely ascribed to the higher substrate temperature during crystallization of the droplet and deposition of the barrier layer surrounding the QD, which therefore provides better material quality as opposed to approaches relying on post-growth annealing.[30,31]

While these numbers still do not reach the Fourier limit, which we will show to be 3 μeV at most, we recall that the reported measurements are performed under above barrier excitation and resonant excitation schemes might be required to suppress charge noise.[44,46] It is, however, worth to point out that such a small level of dephasing is not expected to affect entanglement fidelity.[7]

As required for building up an artificial-natural atomic interface based on Rb, a fraction of the emitters matches the 780 nm spectral window (see Supporting Information for ensemble PL data). Spatial mapping over a 100 x 100 μm^2 area revealed more than 50 emitters with a neutral exciton line with a spectral distance of less than 2 nm from 780 nm. In this wavelength range, a simple external tuning technique would certainly allow precise matching with the Rb transitions. If required, the spatial density of the nanostructures can be further modified during the Ga droplet deposition step independently from their geometry.[16,47] Both ensemble and individual QD optical properties have been probed across the sample on a length scale of the order of 10 mm and displayed good uniformity.

An estimate of the FSS is obtained by mapping the energy position of the exciton and biexciton lines at different linear polarization angles[46] (see Supporting Information for a

typical measurement). The measured FSS values for exciton lines above 770 nm are reported in Fig. 2(c). The average FSS is strongly reduced as compared to DE on (100) substrates[37] with a very low average value of 4.5 μeV and a standard deviation of 3.1 μeV. Moreover, the emitting dipole shows no preferential in-plane orientation, a direct consequence of the improved in-plane symmetry of the QDs presented here (see Fig. 1). Unlike the case of (100) orientation, where an anisotropy in Ga diffusivity systematically causes an in-plane elongation, nanocrystals grown on a (111)A substrate have the C_{3v} symmetry required to achieve vanishing FSS.[25,26] The average FSS value is also more than halved as compared to the best achievement of DE on (111)A substrates up to date.[20] A possible explanation is that the symmetry of the confinement potential is higher in our QDs, because they are thicker and their overall shape is less affected by the accidental presence of underlying monolayer step fluctuations of the substrate. In addition, it has been shown experimentally and theoretically that for a given QD shape, the FSS decreases with increasing dot size and hence decreasing confinement.[48] The reason is that the strength of the exchange interaction responsible for the FSS decreases as the carrier wavefunctions get more delocalized in large QDs (or - in our case - due to the reduced band-offset between barrier and QD material). More generally, this result is state of the art for epitaxial systems on which entangled photon emission has been observed without the need for external tuning.[10,12,13,20,49,50]

Besides the values of the FSS, another important parameter involved in the degree of entanglement is the lifetime of optical transitions. More specifically, the fidelity to the expected Bell state as measured in a time-average experiment depends dramatically on the ratio between the FSS and the exciton lifetime.[14] For this reason, we performed time-resolved measurements on the same sample. Figure 2(d) shows the time decay of the PL intensity of a neutral exciton line under above-barrier excitation. The excitation power was tuned below the saturation level of the exciton in order to prevent band filling effects.[51] In such conditions, the experimental data can be described by the convolution of the instrument response function with a single exponential decay. We approximate the radiative lifetime to

the total decay time of the system, since, in a high quality epitaxial QD at low temperature, non-radiative mechanisms are expected to be negligible.[40,52] We expect an overestimation caused by the contribution to the measured total decay time from the relaxation processes that populate the exciton, so that faster radiative recombination can be achieved by means of resonant excitation (see below). The radiative lifetime has been evaluated over a series of several different QDs and a short average value of 300 ps (with a standard deviation of 60 ps, 20 ps uncertainty on the single measure) was found. This quantity depends rather weakly on emission wavelength (as shown in the Supporting Information). Our values are shorter than those typical of In(Ga)As QDs,[12,53–55] dots embedded in InP nanowires[13] and previous reports of DE GaAs QDs,[20,31] and they are close to the best figures measured on droplet etching GaAs QDs under quasi-resonant excitation.[56]

Thanks to the short radiative lifetime and low FSS, the conditions for polarization-entangled photon emission can be readily met. As mentioned, having at hand the values of the lifetime and FSS for each specific QD is possible to evaluate quantitatively the expected entanglement fidelity, taking into account the measured value of the autocorrelation function (see Supporting Information) and, most importantly, the depolarization effects caused by the hyperfine interaction. Hudson et al.[7] proposed a model for the phase evolution of the exciton-photon intermediate state of the XX-X decay cascade, which leads to Eq. 1 for the fidelity to the expected Bell state.

$$f = \frac{1}{4}\left(1 + \kappa g^{(1)}_{H,V} + \frac{2\kappa g^{(1)}_{H,V}}{1 + \left(g^{(1)}_{H,V} S\tau_1/\hbar\right)^2}\right) \tag{1}$$

In Eq. 1 κ is the fraction of photons generated from the QD exciton with respect to background noise, S is the FSS, τ_1 is the radiative lifetime of the exciton, and $g^{(1)}_{H,V}$ is the first-order cross-coherence. Here we have assumed that cross dephasing is negligible, hence the first-order cross-coherence is given by $g^{(1)}_{H,V} = 1/(1 + \tau_1/\tau_{SS})$, where τ_{SS} is the characteristic time of spin scattering. The κ coefficient can be inferred from autocorrelation measurements as

$\kappa = 1 - g^{(2)}(0)$, with a measured value of exciton $g^{(2)}(0)$ equal to 0.03 ± 0.01. Very recently, Huber et al. (see Supplementary Material of Ref. 14) have demonstrated that by using typical spin scattering time from the literature,[57] the fidelity closely followed the experimental results obtained for droplet etched QDs. Analogous conclusions were drawn in Ref. 50. Following a similar approach, we can calculate the expected fidelity distribution of our QDs obtained by droplet epitaxy, and we find that the large majority of the QDs, over 95%, are potentially able to emit photon pairs with fidelity above the classical limit of 0.5.

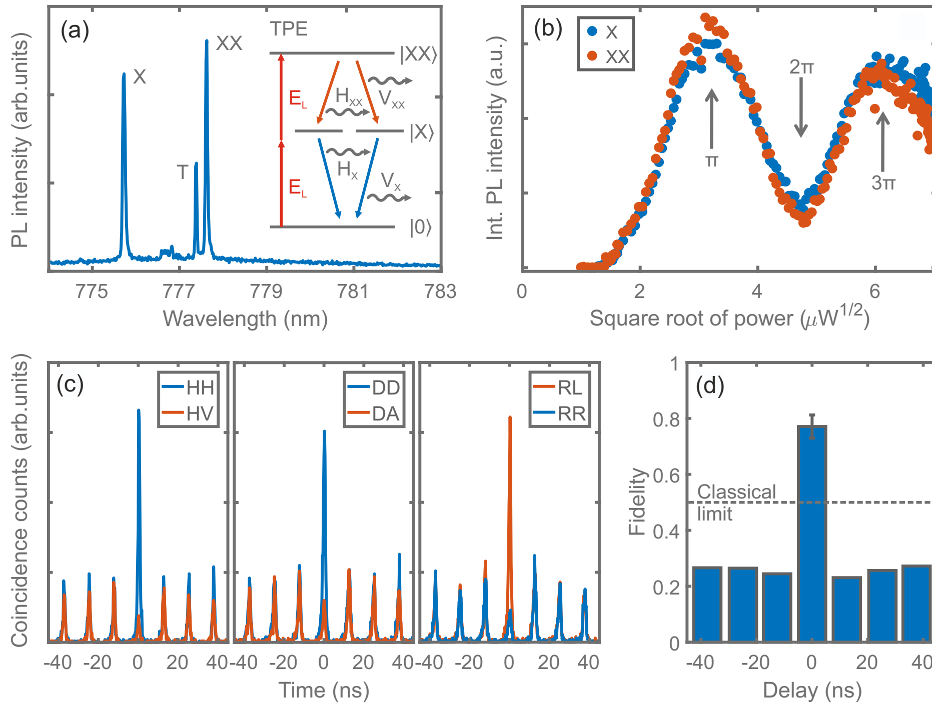

Figure 3: a) Emission spectrum of a single QD under two-photon resonant excitation (TPE). The inset describes the TPE process and the subsequent XX-X cascade. b) Integrated emission intensity of the exciton and biexciton lines under TPE as a function of the square root of the pump power. Rabi oscillations are highlighted. c) Cross-correlation measurements between X and XX emission for different polarization bases, namely linear, diagonal and circular. d) Fidelity to the maximally entangled state.

Having illustrated that almost all our droplet epitaxy QDs have the potential to be used as entangled photon sources, we now move to the characterization of the degree of entanglement of the emitted photons. Schemes to efficiently pump the biexciton have to be

used, as this transition is hardly visible in above-band excitation conditions (see Fig. 2(a)). We employed a two-photon excitation resonant scheme, in which the energy of the laser is tuned half the way between the exciton and biexciton recombination energies.[58] Figure 3(a) shows how the emission energy spectrum is affected. While a contribution from a trion state is still present, the biexciton peak is as intense as the neutral exciton one. The resonant character of the excitation process is demonstrated by the appearance of Rabi oscillations when the laser power is increased, as shown in Fig. 3(b).

In order to demonstrate the emission of polarization-entangled photons, we tuned the excitaton power to π pulse. We considered a QD with a FSS of 2.6 $\pm$ 0.5 μeV, which is a value representative of a significant fraction of the QDs, and a radiative lifetime of 230 ps under resonant excitation. According to Eq. 1, it should provide an entanglement fidelity of 0.77, above the classical limit. The cross-correlation measurements for this QD are shown in Fig. 3(c). Coincidences between the exciton and biexciton lines were counted in three different polarization bases, namely two pairs of orthogonal linear polarizations (H/V and D/A, where D is rotated by 45° with respect to H) in addition to right (R) and left (L) handed circular polarization. The degree of correlation is calculated as $C_{AB} = (g_{XX,X} - g_{XX,\bar{X}})/(g_{XX,X} + g_{XX,\bar{X}})$, where $g_{XX,X}$ and $g_{XX,\bar{X}}$ are the coincidence counts between the exciton and biexciton emission, respectively for co-polarized and cross-polarized photons, integrated over the time window of a single pulse with a time bin of 6 ns. These data directly allow to estimate the fidelity to the expected maximally entangled Bell state[7] according to Eq. 2.

$$f = (1 + C_{HV} + C_{DA} + C_{RL})/4 \tag{2}$$

The fidelity of the zero delay pulse is 0.77 ± 0.04 (error estimated with Gaussian propagation, assuming a Poissonian distribution of the correlation counts), which is significantly above the upper limit for classically correlated states (see Fig. 3(d)). The result is quantitatively consistent with the predictions of the previously discussed X states phase evolution model for GaAs QDs,[14] thus confirming that almost any QD in the ensemble is capable of delivering

entangled photons with fidelities above the classical limit.

In conclusion, we have developed a novel class of droplet epitaxy QDs that can be used as source of entangled photons in the spectral region of the D_2 lines of a cloud of Rb atoms.

The wide applicability of the DE growth scheme allowed us to choose the GaAs/AlGaAs materials system, and to show that 95% of the emitters are capable to deliver photon pairs deterministically and with a fidelity to the expected Bell state above the classical limit.

To achieve this result we dealt with the main drawbacks of conventional DE by introducing droplet crystallization and barrier deposition at high temperature, close to the one used for high quality AlGaAs and GaAs deposition on (111)A. We have shown that this approach improves crystalline quality, leading to reduced spectral wandering and to reliable tuning of the emission wavelength, thanks to limited interdiffusion during the capping process.

As this technology is compatible with integration in optical microcavities for enhanced light extraction, and the growth can be easily adapted to different materials, it has the potential to become an ideal candidate for semiconductor-based sources of entangled photons.

Samples fabrication

The samples were grown in a Gen II molecular beam epitaxy system with an Arsenic valved cracker cell with a base pressure of 10^{-10} torr on intrinsic GaAs (111)A substrates. After the oxide desorption, a 100 nm GaAs buffer layer was deposited at 520°C with a Ga flux of 0.07 ML/s and a beam equivalent pressure of As of 3×10^{-5} torr. Then an AlGaAs barrier with 50 nm of $Al_{0.3}Ga_{0.7}As$ and 100 nm $Al_{0.15}Ga_{0.85}As$ was grown with total group-III fluxes of 0.1 and 0.082 ML/s respectively. For both the buffer and barrier layers the set of parameters for temperature and III-V fluxes were chosen in order to minimize the formation of hillocks and provide flat AlGaAs surface before the QD deposition.[59]

The Ga droplets were formed by depositing 0.4 MLs of Ga with a rate of 0.01 ML/s at 450°C with a background pressure of less than 2×10^{-9} *torr and then removing the sample from the chamber.* The GaAs QDs were formed by depositing 0.4 MLs of Ga with a rate of

0.01 ML/s at 450°C with a background pressure of less than 2×10^{-9} torr and then supplying an As flux with beam equivalent pressure of 3×10^{-5} torr at a substrate temperature of 500°C. The QDs were then covered with a thin layer of $Al_{0.15}Ga_{0.85}As$ grown at 500°C followed by 100 nm $Al_{0.15}Ga_{0.85}As$, 50 nm of $Al_{0.3}Ga_{0.7}As$ and a GaAs capping layer deposited at 520°C. The QD capping procedure was not performed on samples used for morphological characterization, which was carried out by an AFM in tapping mode using ultra sharp tips with a 2 nm radius.

Optical spectroscopy

The sample was mounted inside a low-vibration continuous-flow helium cryostat working at 8 K.

Under non-resonant excitation, single dot PL was excited by a 532 nm continuous wave laser at normal incidence through a 0.42 NA objective. A spatial filter, implemented with a single mode optical fiber, was occasionally added to the collection path to isolate single emitters. The signal was sent to a double grating spectrometer, equipped with 1200 l/mm gratings, which let us achieve a 40 μeV spectral resolution in the 700-800 nm wavelength region, and finally acquired by a deep depletion, back-illuminated, LN2-CCD camera.

Polarization-dependent spectra were acquired by adding a fixed linear polarizer and a rotating half-wave plate to the collection path. FSS was estimated as described in Ref. 37, resulting in an accuracy down to 1 μeV.

Michelson setup and details on the coherence time measurements are provided in Ref. 45.

During time-resolved experiments, the QDs were excited with a pulsed diode laser emitting at 440 nm and their signal was detected by a single photon avalanche detector with time resolution slightly above 50 ps.

Resonant two-photon excitation was accomplished using a Ti:sapphire femtosecond laser. The pulse duration was broadened from 100 fs to about 10 ps by means of a 4f pulse-shaper.

Tunable notch filters with a bandwidth of 0.4 nm were placed in the collection path to suppress laser backscattering.

Photon correlation experiments were performed with a Hanbury-Brown-Twiss setup. The signal collected from the objective was sent to a non-polarizing beamsplitter and then to two polarization maintaining single mode fibers. The PL signal at the output of these fibers was sent to two independent spectrometers which could be tuned to direct a specific wavelength to an avalanche photodiode. The avalanche detectors were connected to the correlation electronics and each provided 500 ps timing jitter. For the fidelity measurement, exciton-biexciton cross-correlation was measured in different polarization bases, selected by linear polarizers and half- or quarter-wave plates inserted right after the beamsplitter.

Acknowledgement

This work was financially supported by the European Research council (ERC) under the European Union's Horizon 2020 Research and Innovation Programme (SPQRel, Grant Agreement No. 679183). This project has received funding from the European Union's Horizon 2020 research and innovation programme under the Marie Skłodowska-Curie grant agreement No. 721394. We thank Emanuele Grilli for fruitful discussions.

Supporting Information Available

Contour AFM map of a single QD. Ensemble photoluminescence. Lifetime and FSS data collected at different emission wavelengths. Typical polarization-resolved measurement and power-dependent analysis of single dot PL. Experimental autocorrelation function for X and XX emission.

This material is available free of charge via the Internet at `http://pubs.acs.org/`.

References

(1) Kimble, H. J. *Nature* **2008**, *453*, 1023–1030.

(2) Pan, J.-W.; Chen, Z.-B.; Lu, C.-Y.; Weinfurter, H.; Zeilinger, A.; Żukowski, M. *Rev. Mod. Phys.* **2012**, *84*, 777–838.

(3) Benson, O.; Santori, C.; Pelton, M.; Yamamoto, Y. *Phys. Rev. Lett.* **2000**, *84*, 2513–2516.

(4) Lu, C.-Y.; Pan, J.-W. *Nature Photonics* **2014**, *8*, 174–176.

(5) Bester, G.; Nair, S.; Zunger, A. *Phys. Rev. B* **2003**, *67*, 161306.

(6) Seguin, R.; Schliwa, A.; Rodt, S.; Pötschke, K.; Pohl, U. W.; Bimberg, D. *Phys. Rev. Lett.* **2005**, *95*, 257402.

(7) Hudson, A. J.; Stevenson, R. M.; Bennett, A. J.; Young, R. J.; Nicoll, C. A.; Atkinson, P.; Cooper, K.; Ritchie, D. A.; Shields, A. J. *Phys. Rev. Lett.* **2007**, *99*, 266802.

(8) Treu, J.; Schneider, C.; Huggenberger, A.; Braun, T.; Reitzenstein, S.; Höfling, S.; Kamp, M. *Applied Physics Letters* **2012**, *101*.

(9) Mano, T.; Abbarchi, M.; Kuroda, T.; McSkimming, B.; Ohtake, A.; Mitsuishi, K.; Sakoda, K. *Applied Physics Express* **2010**, *3*, 065203.

(10) Huo, Y. H.; Rastelli, A.; Schmidt, O. G. *Applied Physics Letters* **2013**, *102*, 152105.

(11) Yerino, C. D.; Simmonds, P. J.; Liang, B.; Jung, D.; Schneider, C.; Unsleber, S.; Vo, M.; Huffaker, D. L.; Höfling, S.; Kamp, M.; Lee, M. L. *Applied Physics Letters* **2014**, *105*.

(12) Juska, G.; Dimastrodonato, V.; Mereni, L. O.; Gocalinska, A.; Pelucchi, E. *Nat. Photon.* **2013**, *7*, 527.

(13) Versteegh, M. A. M.; Reimer, M. E.; Jöns, K. D.; Dalacu, D.; Poole, P. J.; Gulinatti, A.; Giudice, A.; Zwiller, V. *Nat. Commun.* **2014**, *5*, 5298.

(14) Huber, D.; Reindl, M.; Huo, Y.; Huang, H.; Wildmann, J.; Schmidt, O.; Rastelli, A.; Trotta, R. *Nature Communications* **2017**, *8*, 15506.

(15) Sanguinetti, S.; Koguchi, N. In *Molecular Beam Epitaxy: From Research to Mass Production*; Henini, M., Ed.; Elsevier: Oxford, 2013; p 95.

(16) Heyn, C.; Stemmann, A.; Schramm, A.; Welsch, H.; Hansen, W.; Nemcsics, A. *Phys. Rev. B* **2007**, *76*, 075317.

(17) Bietti, S.; Bocquel, J.; Adorno, S.; Mano, T.; Keizer, J. G.; Koenraad, P. M.; Sanguinetti, S. *Phys. Rev. B* **2015**, *92*, 075425.

(18) Liu, X.; Ha, N.; Nakajima, H.; Mano, T.; Kuroda, T.; Urbaszek, B.; Kumano, H.; Suemune, I.; Sakuma, Y.; Sakoda, K. *Phys. Rev. B* **2014**, *90*, 081301.

(19) Skiba-Szymanska, J.; Stevenson, R. M.; Varnava, C.; Felle, M.; Huwer, J.; Müller, T.; Bennett, A. J.; Lee, J. P.; Farrer, I.; Krysa, A. B.; Spencer, P.; Goff, L. E.; Ritchie, D. A.; Heffernan, J.; Shields, A. J. *Phys. Rev. Applied* **2017**, *8*, 014013.

(20) Kuroda, T.; Mano, T.; Ha, N.; Nakajima, H.; Kumano, H.; Urbaszek, B.; Jo, M.; Abbarchi, M.; Sakuma, Y.; Sakoda, K.; Suemune, I.; Marie, X.; Amand, T. *Phys. Rev. B* **2013**, *88*, 041306.

(21) Stevenson, R. M.; Young, R. J.; Atkinson, P.; Cooper, K.; Ritchie, D. A.; Shields, A. J. *Nature* **2006**, *439*, 179–182.

(22) Bennett, A.; Pooley, M.; Stevenson, R.; Ward, M.; Patel, R.; de La Giroday, A. B.; Sköld, N.; Farrer, I.; Nicoll, C.; Ritchie, D.; Shields, A. *Nature Physics* **2010**, *6*, 947–950.

(23) Trotta, R.; Martín-Sánchez, J.; Wildmann, J. S.; Piredda, G.; Reindl, M.; Schimpf, C.; Zallo, E.; Stroj, S.; Edlinger, J.; Rastelli, A. *Nature Communications* **2016**, *7*, 10375.

(24) Muller, A.; Fang, W.; Lawall, J.; Solomon, G. S. *Phys. Rev. Lett.* **2009**, *103*, 217402.

(25) Singh, R.; Bester, G. *Phys. Rev. Lett.* **2009**, *103*, 063601.

(26) Schliwa, A.; Winkelnkemper, M.; Lochmann, A.; Stock, E.; Bimberg, D. *Phys. Rev. B* **2009**, *80*, 161307.

(27) Akopian, N.; Wang, L.; Rastelli, A.; Schmidt, O.; Zwiller, V. *Nature Photonics* **2011**, *5*, 230–233.

(28) Huang, H.; Trotta, R.; Huo, Y.; Lettner, T.; Wildmann, J. S.; Martín-Sánchez, J.; Huber, D.; Reindl, M.; Zhang, J.; Zallo, E.; Schmidt, O. G.; Rastelli, A. *ACS photonics* **2017**, *4*, 868–872.

(29) Patel, R. B.; Bennett, A. J.; Farrer, I.; Nicoll, C. A.; Ritchie, D. A.; Shields, A. J. *Nature Photonics* **2010**, *4*, 632–635.

(30) Mantovani, V.; Sanguinetti, S.; Guzzi, M.; Grilli, E.; Gurioli, M.; Watanabe, K.; Koguchi, N. *Journal of Applied Physics* **2004**, *96*, 4416–4420.

(31) Mano, T.; Abbarchi, M.; Kuroda, T.; Mastrandrea, C.; Vinattieri, A.; Sanguinetti, S.; Sakoda, K.; Gurioli, M. *Nanotechnology* **2009**, *20*, 395601.

(32) Jo, M.; Mano, T.; Abbarchi, M.; Kuroda, T.; Sakuma, Y.; Sakoda, K. *Crystal Growth & Design* **2012**, *12*, 1411–1415.

(33) Watanabe, K.; Tsukamoto, S.; Gotoh, Y.; Koguchi, N. *Journal of crystal growth* **2001**, *227*, 1073–1077.

(34) Sato, K.; Fahy, M.; Joyce, B. *Surface Science* **1994**, *315*, 105 – 111.

(35) Scarpellini, D.; Fedorov, A.; Somaschini, C.; Frigeri, C.; Bollani, M.; Bietti, S.; Nötzel, R.; Sanguinetti, S. *Nanotechnology* **2017**, *28*, 045605.

(36) Bietti, S.; Somaschini, C.; Esposito, L.; Fedorov, A.; Sanguinetti, S. *Journal of Applied Physics* **2014**, *116*, 114311.

(37) Abbarchi, M.; Mastrandrea, C. A.; Kuroda, T.; Mano, T.; Sakoda, K.; Koguchi, N.; Sanguinetti, S.; Vinattieri, A.; Gurioli, M. *Phys. Rev. B* **2008**, *78*, 125321.

(38) Luo, J.-W.; Zunger, A. *Phys. Rev. B* **2011**, *84*, 235317.

(39) Juska, G.; Murray, E.; Dimastrodonato, V.; Chung, T. H.; Moroni, S. T.; Gocalinska, A.; Pelucchi, E. *Journal of Applied Physics* **2015**, *117*, 134302.

(40) Jahn, J.-P.; Munsch, M.; Béguin, L.; Kuhlmann, A. V.; Renggli, M.; Huo, Y.; Ding, F.; Trotta, R.; Reindl, M.; Schmidt, O. G.; Rastelli, A.; Treutlein, P.; Warburton, R. J. *Phys. Rev. B* **2015**, *92*, 245439.

(41) Uskov, A. V.; Magnusdottir, I.; Tromborg, B.; Mørk, J.; Lang, R. *Applied Physics Letters* **2001**, *79*, 1679–1681.

(42) Ha, N.; Mano, T.; Chou, Y.-L.; Wu, Y.-N.; Cheng, S.-J.; Bocquel, J.; Koenraad, P. M.; Ohtake, A.; Sakuma, Y.; Sakoda, K.; Kuroda, T. *Phys. Rev. B* **2015**, *92*, 075306.

(43) Berthelot, A.; Favero, I.; Cassabois, G.; Voisin, C.; Delalande, C.; Roussignol, P.; Ferreira, R.; Gérard, J.-M. *Nature Physics* **2006**, *2*, 759–764.

(44) Kuhlmann, A. V.; Houel, J.; Ludwig, A.; Greuter, L.; Reuter, D.; Wieck, A. D.; Poggio, M.; Warburton, R. J. *Nature Physics* **2013**, *9*, 570–575.

(45) Kammerer, C.; Cassabois, G.; Voisin, C.; Perrin, M.; Delalande, C.; Roussignol, P.; Gérard, J. M. *Applied Physics Letters* **2002**, *81*, 2737–2739.

(46) Bayer, M.; Ortner, G.; Stern, O.; Kuther, A.; Gorbunov, A. A.; Forchel, A.; Hawrylak, P.; Fafard, S.; Hinzer, K.; Reinecke, T. L.; Walck, S. N.; Reithmaier, J. P.; Klopf, F.; Schäfer, F. *Phys. Rev. B* **2002**, *65*, 195315.

(47) Ohtake, A.; Ha, N.; Mano, T. *Crystal Growth & Design* **2015**, *15*, 485–488.

(48) Huo, Y. H.; Křápek, V.; Rastelli, A.; Schmidt, O. G. *Physical Review B* **2014**, *90*, 041304.

(49) Young, R. J.; Stevenson, R. M.; Shields, A. J.; Atkinson, P.; Cooper, K.; Ritchie, D. A.; Groom, K. M.; Tartakovskii, A. I.; Skolnick, M. S. *Phys. Rev. B* **2005**, *72*, 113305.

(50) Keil, R.; Zopf, M.; Chen, Y.; Höfer, B.; Zhang, J.; Ding, F.; Schmidt, O. G. *Nature Communications* **2017**, *8*, 15501.

(51) Raymond, S.; Fafard, S.; Poole, P. J.; Wojs, A.; Hawrylak, P.; Charbonneau, S.; Leonard, D.; Leon, R.; Petroff, P. M.; Merz, J. L. *Phys. Rev. B* **1996**, *54*, 11548–11554.

(52) Tighineanu, P.; Daveau, R.; Lee, E. H.; Song, J. D.; Stobbe, S.; Lodahl, P. *Phys. Rev. B* **2013**, *88*, 155320.

(53) Dalgarno, P. A.; Smith, J. M.; McFarlane, J.; Gerardot, B. D.; Karrai, K.; Badolato, A.; Petroff, P. M.; Warburton, R. J. *Phys. Rev. B* **2008**, *77*, 245311.

(54) Langbein, W.; Borri, P.; Woggon, U.; Stavarache, V.; Reuter, D.; Wieck, A. D. *Phys. Rev. B* **2004**, *70*, 033301.

(55) Trotta, R.; Wildmann, J. S.; Zallo, E.; Schmidt, O. G.; Rastelli, A. *Nano Letters* **2014**, *14*, 3439–3444.

(56) Akopian, N.; Trotta, R.; Zallo, E.; Kumar, S.; Atkinson, P.; Rastelli, A.; Schmidt, O.; Zwiller, V. *arXiv preprint arXiv:1302.2005* **2013**,

(57) Chekhovich, E.; Makhonin, M.; Tartakovskii, A.; Yacoby, A.; Bluhm, H.; Nowack, K.; Vandersypen, L. *Nature materials* **2013**, *12*, 494–504.

(58) Müller, M.; Bounouar, S.; Jöns, K. D.; Glässl, M.; Michler, P. *Nature Photonics* **2014**, *8*, 224–228.

(59) Esposito, L.; Bietti, S.; Fedorov, A.; Nötzel, R.; Sanguinetti, S. *Phys. Rev. Materials* **2017**, *1*, 024602.

Graphical TOC Entry